Chemical Engineering Research and Design 203 (2024) 453–466

Contents lists available at ScienceDirect

Chemical Engineering Research and Design

journal homepage: www.elsevier.com/locate/cherd

Insulin nucleation kinetics in an oscillatory flow-based platform: Protein crystallization as a highly reproducible separation process

Joana Ferreira [a,b,*], Sofia Araújo [b,c], António Ferreira [b,c], José Teixeira [d,e], João Moreira de Campos [a,b], Fernando Rocha [b,c], Filipa Castro [b,c]

[a] CEFT – Transport Phenomena Research Center, Department of Chemical Engineering, Faculty of Engineering, University of Porto, Rua Dr. Roberto Frias, 4200-465 Porto, Portugal
[b] ALiCE – Associate Laboratory in Chemical Engineering, Faculty of Engineering, University of Porto, Rua Dr. Roberto Frias, 4200-465 Porto, Portugal
[c] LEPABE – Laboratory for Process Engineering, Environment, Biotechnology and Energy, Faculty of Engineering, University of Porto, Rua Dr. Roberto Frias, 4200-465 Porto, Portugal
[d] CEB – Centre for Biological Engineering, University of Minho, Campus de Gualtar, 4710-057 Braga, Portugal
[e] LABBELS – Associate Laboratory in Biotechnology, Bioengineering and Microelectromechanical Systems, University of Minho, Campus de Gualtar, 4710-057 Braga, Portugal

ARTICLE INFO

Keywords:
Insulin
Nucleation kinetics
Crystallization
Oscillatory Flow Reactor

ABSTRACT

Insulin is a human therapeutic protein that has been used to treat diabetes for almost a century. Its crystallization has been of significant interest since the protein is commonly administered by subcutaneous injections of crystalline formulations, where crystal size distribution (CSD) has a critical role in product release and injectability. Herein, insulin crystallization was investigated in a unique platform based on oscillatory flow mixing technology. Assays were carried out at different supersaturation ratios (*i.e.*, insulin concentrations) in the presence and absence of acetone, and turbidity of the crystallization solution was monitored over time by UV-Vis spectrophotometry. The results show the impact of both supersaturation ratio and acetone on nucleation kinetics, as well as on CSD and growth rate. As the initial supersaturation increases, the nucleation rate increases, and the growth rate and mean crystal size decrease. The presence of acetone allows a faster nucleation event, a narrower CSD and a larger mean crystal size. The kinetic parameter *A* derived from the *Classical Nucleation Theory* (CNT) also indicates the kinetics of molecular attachment acceleration in the presence of acetone. These findings contribute to a better understanding of insulin crystallization processes under oscillatory flow. Thus, the described strategy and oscillatory flow-based systems are very promising for optimizing protein crystallization processes to be used during the downstream separation of bioproducts.

1. Introduction

In line with the *World Health Organization*'s (WHO) report from last year (WHO. World Health Statistics, 2023), there is a growing demand for therapeutics owing to an increased incidence of chronic diseases (*e.g.*, diabetes, cancer), as well as the need for novel therapies to the treatment of rare genetic and infectious diseases (Agyei et al., 2017). Advances in upstream technologies (fermentation and cell culture) have significantly increased proteins product titers (dos Santos et al., 2017). Those improvements have shifted the manufacturing bottleneck towards downstream processing (DSP), which can contribute up to 80% of the total production costs (dos Santos et al., 2017; Roque et al., 2020). DSP usually involves several sequential chromatographic steps associated with high operating costs and limited throughput due to inherent transfer phenomena limitations (dos Santos et al., 2017; Hekmat, 2015; Roque et al., 2020), and, consequently, more cost-effective DSP approaches are required.

Biomacromolecular crystallization has mostly been exploited to obtain structural information by X-ray crystallography (dos Santos et al., 2017). However, it is also of extraordinary value in DSP. Contrarily to chromatography, protein crystallization (1) requires no costly equipment and consumables (*e.g.*, resins), (2) handles high process volumes and protein titers, and (3) yields highly pure suspensions in a single step (Castro et al., 2022b; dos Santos et al., 2017; Hekmat, 2015; Roque et al.,

* Corresponding author at: CEFT – Transport Phenomena Research Center, Department of Chemical Engineering, Faculty of Engineering, University of Porto, Rua Dr. Roberto Frias, 4200-465 Porto, Portugal.
E-mail address: jmpferreira@fe.up.pt (J. Ferreira).

https://doi.org/10.1016/j.cherd.2024.01.057
Received 10 November 2023; Received in revised form 20 January 2024; Accepted 29 January 2024
Available online 1 February 2024

2020). Additionally, crystalline proteins offer advantages in terms of product activity, stability, and control of drug release when compared to their liquid forms (Hekmat, 2015; Puhl et al., 2016).

Although crystallization is widely applied to small organic molecules (*e.g.*, pharmaceuticals) (Chen et al., 2011), there has been limited development in the industrial implementation of biopharmaceutical crystallization. The development of protein crystallization operations is primarily based on empirical approaches. This fact is mainly due to a limited understanding of the underlying phenomena, such as the stochastic nature of (primary) nucleation (García-Ruiz, 2003) and the peculiarities of protein-protein interactions (McPherson and Gavira, 2014; Nanev, 2020; Price et al., 2010). On the one hand, proteins are large, complex, and dynamic molecules, and beyond that, their physical properties are intimately related to their surrounding environment (McPherson and Gavira, 2014). On the other hand, the interactions between protein surfaces driving crystallization are weak, complex, and non-covalent (Price et al., 2010). Therefore, there is poor control over the protein crystallization process (*e.g.*, yield, process cost, operation time) and outcome variables (*e.g.*, crystal size, shape, morphology).

Insulin is the first crystalline protein approved for therapeutic uses (*i.e.*, diabetes treatment). This therapeutic protein has predominantly been administered by subcutaneous injections, where crystal size distribution (CSD) is critical in product release and injectability (Basu et al., 2004). Thus, insulin crystallization is a topic of great interest with promising perspectives. Most works on insulin crystallization have been carried out at the microscale and under static conditions. These reported studies mostly focus on thermodynamics (Bergeron et al., 2003), kinetics (Nanev et al., 2011b; Nanev, 2013; Nanev and Tonchev, 2015; Reviakine et al., 2003), control of the nucleation process (Ferreira et al., 2022b; Hodzhaoglu et al., 2016; Li and Lakerveld, 2017; Link and Heng, 2021), and reduction of crystal size polydispersity (Nanev et al., 2013; Nanev and Petrov, 2017; Tonchev and Nanev, 2013). However, there is the lack of a standardized protocol to crystallize insulin. Several protocols are reported with distinct conditions, such as buffer, precipitating agent, or even additives and co-solvents at distinct protein concentration, pH, and temperature ranges. Besides these aspects, there are few investigations on insulin crystallization at the milliliter scale. The published works assess insulin crystallization in different flow systems, including static conditions (Bernardo et al., 2004; Link and Heng, 2022; Penkova et al., 2004), stirred vessels (Hirata et al., 2012, 2010), oscillatory flow (Parambil et al., 2011), sheared flow (Ferreira et al., 2022a) and smoothed-oscillatory flow (Araújo, 2022) in batch mode, as well as segmented flow in continuous mode (Chen et al., 2021). However, crystallization kinetics data, especially nucleation kinetics, still lack in the literature.

Mixing efficiency is a critical factor for the success of crystallization processes because it significantly affects process reproducibility and product quality (*e.g.*, CSD). A homogeneous mixture is required to achieve a uniform supersaturation distribution, while minimizing crystal attrition and, hence, secondary nucleation (Hekmat, 2015; Mullin, 2001). Recently, oscillatory flow reactors with smooth periodic constrictions (OFR-SPC) (Ferreira et al., 2019, 2016a, 2016b) have stood out in the process intensification of multiphase systems, from gas-liquid mass transfer (Almeida et al., 2022; Ferreira et al., 2015; Gonçalves et al., 2021; Graça et al., 2020) to API crystallization (Cruz et al., 2018, 2016) and protein crystallization (Castro et al., 2022a, 2018, 2016) applications. The fluid flow along the periodic constrictions results in vortices and eddies formation, thus providing a high mixing efficiency. Contrarily to stirred vessels with impellers that may easily induce attrition (Hekmat, 2015), and tubular crystallizers prone to fouling and clogging (Mathew Thomas et al., 2022), OFR-SPC offers a singular geometry and mixing mechanism, which allow a reduction of high shear regions and increase of crystal suspension. In addition, the mixing intensity can be varied by tuning the oscillation conditions [*i.e.*, oscillation frequency (f) and amplitude (x_0)] and enabling different flow regimes (from laminar to turbulent) (Pereira, 2017).

Limited research has been conducted on insulin crystallization under oscillation, particularly exploring crystallization kinetics. Furthermore, there is a lack of standardized protocols to crystallize insulin regardless of the studied crystallizer type and scale. In this context, this work presents a unique platform based on oscillatory flow technology for investigation and *in-line* monitoring of protein crystallization experiments. Following the previous crystallization studies of the research group (Araújo, 2022; Ferreira et al., 2022b, 2022a), insulin batch crystallization assays were carried out in a meso scale OFR-SPC coupled to a spectrometer for *in-situ* measurements of solution turbidity. Herein, the influence of insulin concentration and presence of acetone on nucleation kinetics and CSD were assessed. Lastly, induction times were estimated, and nucleation rates were calculated following the validity of the *Classical Nucleation Theory* (CNT), while growth rates were experimentally measured and empirically predicted. CSD was determined from optical microscopy images of crystalline suspensions.

2. Materials and methods

2.1. Crystallization solutions preparation and solubility analysis

The crystallization solutions were prepared according to the protocol reported by Ferreira et al. (2022b). Doubled concentrated recombinant human insulin (Sigma-Aldrich, 5808 g·mol^{-1}, CAS No. 11061-68-0, Lot. No. 20E304) and precipitant solutions were prepared in a highly diluted hydrochloric acid (HCl) (37%, Chem-Lab Analytical, CAS-No. 7647-01-0) solution (20 mM). The HCl solution was prepared with ultrapure water (Milli Q water, resistivity of 18.3 MΩ·cm^{-1} at 25 °C). Regarding the preparation of the insulin solution, a suitable amount of insulin powder was weighted and dissolved in HCl (20 mM) to achieve the desired concentration (Table 1). The resulting solution was used without further purification. The precipitant solution was prepared by adding zinc chloride ($ZnCl_2$) (Sigma-Aldrich, CAS-No. 7646–85-7), trisodium citrate (TC) (Sigma-Aldrich, CAS-No. 6132- 04–3), and neat acetone, following this order (Ferreira et al., 2022b), where the concentration of each component in solution was 7.50 mM $ZnCl_2$, 75.0 mM TC and 0% or 30% (v/v) acetone (pH 5.7). Both insulin and precipitant solutions were prepared at room temperature without pre-heating or centrifugation steps. All the solutions were filtered through a syringe filter (Puradisc FP 30 mm, cellulose acetate, 0.2 μm) (Sigma-Aldrich, Whatman) to remove undissolved impurities and amorphous aggregates (Mühlig et al., 2001).

The solubility of insulin was also measured in the presence and/or absence of acetone at the precipitant solution concentration used during the crystallization assays (pH 5.7 and 20 °C). Crystallization solutions were prepared by mixing equal volumes of insulin and precipitant

Table 1
Summary of the initial experimental conditions in the meso OFR-SPC at 20 °C and pH 5.7 in the presence and absence of acetone, where $S_i = C_p^i/C_p^{eq}$.

	Condition	C_p^{eq} [mg·mL^{-1}]	C_p^i [mg·mL^{-1}]	S_i [-]
Acetone	**A1**	0.062 ± 0.007	2.5 ± 0.04	39.9 ± 4.8
	A2		1.2 ± 0.02	20.0 ± 2.4
	A3		0.71 ± 0.06	11.4 ± 1.7
	A4		0.55 ± 0.08	8.8 ± 1.7
	A5		0.25 ± 0.01	4.1 ± 0.5
	A6		0.22 ± 0.01	3.6 ± 0.5
	A7		0.15 ± 0.003	2.4 ± 0.3
No Acetone	**B1**	0.12 ± 0.001	2.5 ± 0.04	20.8 ± 0.04
	B2		1.2 ± 0.02	10.5 ± 0.2
	B3		0.71 ± 0.06	6.0 ± 0.5
	B4		0.55 ± 0.08	4.6 ± 0.7
	B5		0.25 ± 0.01	2.1 ± 0.08
	B6		0.22 ± 0.01	1.9 ± 0.1
	B7		0.15 ± 0.003	1.3 ± 0.03

[The errors are standard deviations from at least three independent experiments].

solutions. The resulting crystallization solutions were stored overnight at 4 °C and afterwards incubated at 20 °C until reaching equilibrium. Each day, after gentle stirring to ensure that the crystals were suspended in the crystallization solution volume, aliquot suspensions were collected. The suspensions were then filtered (0.2 μm) and, if required, diluted for measuring the protein concentration in solution by UV-Vis spectrophotometry. When the protein concentration value stabilized after three consecutive days, the measured protein concentration was assumed to be the equilibrium concentration, *i.e.*, corresponding to the solubility concentration.

2.2. Crystallization experiments

The experimental set-up involves a meso oscillatory flow reactor (OFR) placed vertically [Fig. 1-(1)], a mixing chamber (Push-in T-connector, NPQP-T-Q8-E-FD-P10, Festo) [Fig. 1-(3)], a linear motor (LinMot, HFOI-23, Switzerland) [Fig. 1-(5)], and a measuring cell (Sarspec, Portugal) [Fig. 1-(6)] coupled to a spectrometer (ScanSpec UV-Vis, Sarspec, Portugal) [Fig. 1-(8)] (Fig. 1). The meso OFR consists of a 35 cm long and 3 mm internal diameter glass jacketed tube provided with smooth periodic constrictions (SPC) and has an approximate volume of 4 mL (Ferreira et al., 2019, 2016a, 2016b), which characteristic dimensions are shown in Fig. 1. The insulin and precipitant solutions are fed into the set-up through a syringe pump (NE-4000, New Era, United States of America) [Fig. 1-(2)], using a low flow rate (3 mL·min^{-1}) to avoid the formation of bubbles in the meso OFR-SPC. The mixing intensity is controlled by the oscillation frequency (f) and amplitude (x_0) fixed at 1.83 Hz and 5.3 mm, respectively, which was based on the results of a previous work by Castro et al. (2018). During the study of lysozyme crystallization in a similar meso OFR-SPC, Castro and co-workers found a non-monotonic dependence of both induction time and mean crystal size on mixing intensity, which highlighted the existence of an optimum oscillatory Reynolds number ($Re_o = 2\pi\rho D f x_0/\mu$, where ρ [kg·m^{-3}] is the fluid density, D [m] the internal diameter glass jacketed tube, and μ [Pa·s] the fluid dynamic viscosity) that led to a faster nucleation. The induction time and mean crystal size showed a stronger dependency on the amplitude compared to the frequency, which was probably due to the predominant role of the oscillation amplitude in fluid mixing. The amplitude value corresponds to the center-to-peak amplitude measured in the tube without constrictions. The temperature inside the meso OFR-SPC was controlled by a thermostatic bath (Huber, Ministat 125, Germany) [Fig. 1-(4)].

Isothermal batch insulin crystallization trials were carried out at 20 °C and pH 5.7 for 150 min. Each experiment started by simultaneously injecting equal volumes of insulin and precipitant solutions in the meso OFR-SPC [Fig. 1-(2)]. At least three independent experiments were carried out for each experimental condition (Table 1).

2.3. Insulin crystallization kinetics

2.3.1. Induction time and nucleation kinetics

The solution turbidity was monitored over time through UV-Vis

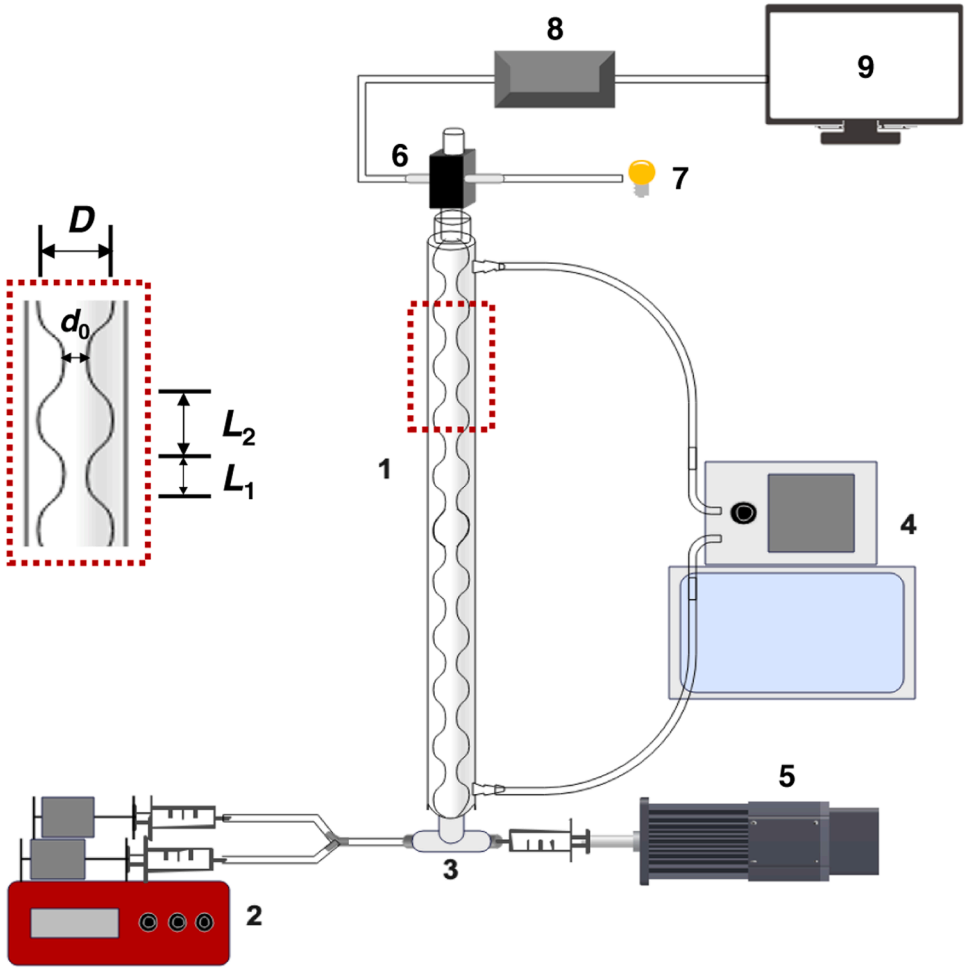

Fig. 1. Schematic representation of the experimental set-up and characteristic dimensions of the meso OFR-SPC: **(1)** OFR-SPC with characteristics dimensions D = 3 mm, d_0 = 1.6 mm, L_1 = 6 mm, and L_2 = 13 mm, **(2)** syringe pump; **(3)** mixing chamber, **(4)** temperature control through a thermostatic bath, **(5)** linear motor, **(6)** measuring cell, **(7)** light source, **(8)** spectrometer, and **(9)** data acquisition.

spectrophotometry (wavelength, $\lambda = 400$ nm) to obtain quantitative insight into the insulin nucleation phenomena. The experimental methodology was based on a previous work (Castro et al., 2016). The induction time (t_{ind}) was estimated from the turbidity (τ) and/or absorbance (Abs) curves [Fig. 2-(a)]. Hence, its experimental determination significantly depends on the employed analytical technique. For the implemented methodology in this study, the estimated induction time corresponds to the time that passes until a significant change in the turbidity of the crystallization solution is detected, *i.e.*, the moment at which the suspension contains a certain volume fraction of crystals as the light transmission is not capable of capturing only nuclei (Brandel and ter Horst, 2015). An increment of 0.017 in turbidity was related to the occurrence of a nucleation event [Fig. 2-(b)]. In this way, the latent period (*i.e.*, the onset of a significant change in the system (Mullin, 2001)) was assessed as a mean of induction time to compare the onset of crystallization for the different studied experimental conditions (Table 1). Although the induction time strongly depends on external factors, it has often been used to measure nucleation kinetics (Bernardo et al., 2004; Brandel and ter Horst, 2015; Jiang and ter Horst, 2011; Mullin, 2001; Shiau, 2022). Lastly, the nucleation probability and nucleation rate were calculated using Eqs. (A1) and (A4) (see Appendix section), respectively.

During the crystallization assays performed at low insulin concentrations (conditions A3–A7 and B5–B7, Table 1), no drastic turbidity changes were registered in the crystallization medium. Consequently, it was not possible to estimate the induction time for these experimental conditions.

2.3.2. Protein concentration

Insulin concentrations were measured by UV-Vis spectrophotometry. The insulin concentration was measured for crystallization trials performed in the absence of acetone at $\lambda = 280$ nm (ScanSpec UV−Vis, Sarspec, Portugal). For the experiments in the presence of acetone, insulin concentration was measured at $\lambda = 562$ nm through Thermo Scientific™ Pierce™ BCA Protein Assay Kit using a multi-detection microplate reader (Synergy™ HT, BioTek Instruments, USA). All the concentration measurements were carried out at least in triplicate. For both cases, calibration curves were measured.

2.3.3. Crystal size distribution (CSD)

The collected suspensions were observed under an optical microscope (Standard 20, Zeiss, Germany) coupled to a camera (Konus 5827 CCD) to measure mean crystal size, CSD, and crystal shape. A minimum of 500 crystals were measured using *Image J* ("ImageJ," 2019) to ensure a representative population of crystals with a 90% confidence interval (Faria et al., 2003). Mean crystal size and CSD were determined by measuring the Feret's diameter. Only single crystals were considered, *i.e.*, aggregated crystals were not accounted for the experimental determination of CSD. Two strategies were used to calculate the growth rate based on experimental (crystal size and total duration of each crystallization trial [$L_c(t)/t$]) and empirical [Eq. (A8)] data.

2.3.4. Crystallization yield

Crystallization yield (η [%]) was estimated based on the measured initial (C_p^i [kg·m^{-3}]) and final (C_p^f [kg·m^{-3}]) protein concentrations in solution as shown by Eq. (1).

$$\eta = \frac{C_p^i - C_p^f}{C_p^i - C_p^{eq}}, \tag{1}$$

where C_p^{eq} [kg·m^{-3}] is the protein equilibrium concentration (solubility concentration).

3. Results and discussion

3.1. Insulin nucleation kinetics

3.1.1. Induction time and nucleation probability

The induction times (t_{ind}) for the crystallization of insulin in the meso OFR-SPC at varying experimental conditions (conditions A1–A2 and B1–B4, Table 1) were experimentally determined. The relationship between t_{ind} and the initial supersaturation ratio (S_i) is shown in Fig. 3. The probability distributions of the induction time [Eq. (A1), see Appendix section] at different initial supersaturation ratios in the presence and absence of acetone are presented in Fig. 4.

For both in the presence (conditions A1–A2, Table 1) and absence (conditions B1–B4, Table 1) of acetone in the crystallization medium, the induction time decreases linearly with the initial supersaturation

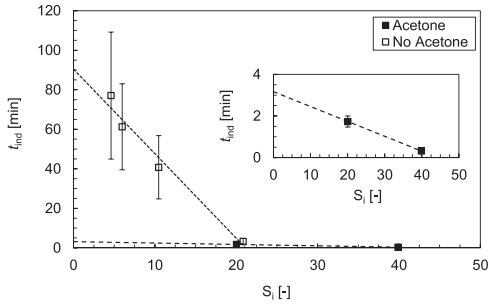

Fig. 3. Experimentally measured induction time as a function of the initial supersaturation ratio for insulin crystallization assays performed in the presence and absence of acetone in the meso OFR-SPC at 20 °C and pH 5.7. The error bars are standard deviations from at least three independent experiments. [Lines are only represented to guide the eye].

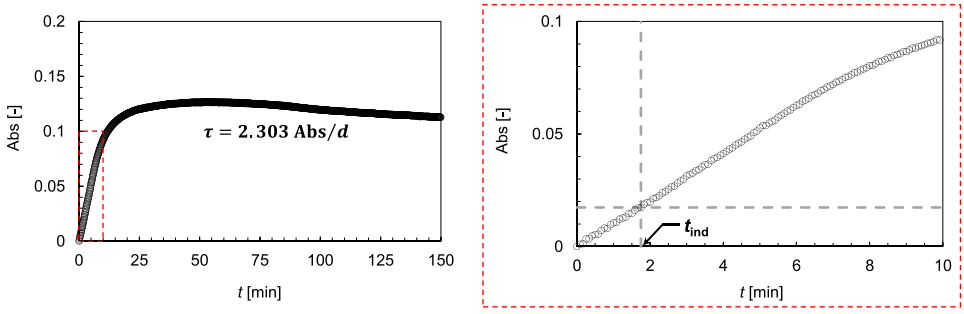

Fig. 2. **(a)** Schematic representation of the implemented methodology to estimate the induction time (t_{ind}) based on the measured absorbance (Abs) over time (t) and, consequently, the determination of the turbidity (τ) applying the highlighted equation (d corresponds to the scattering pathlength, 0.4 cm) (Castro et al., 2016). **(b)** Insert highlighting the absorbance range indicated in (a) and the correspondent absorbance increment (0.017) at which the time interval represents the induction time.

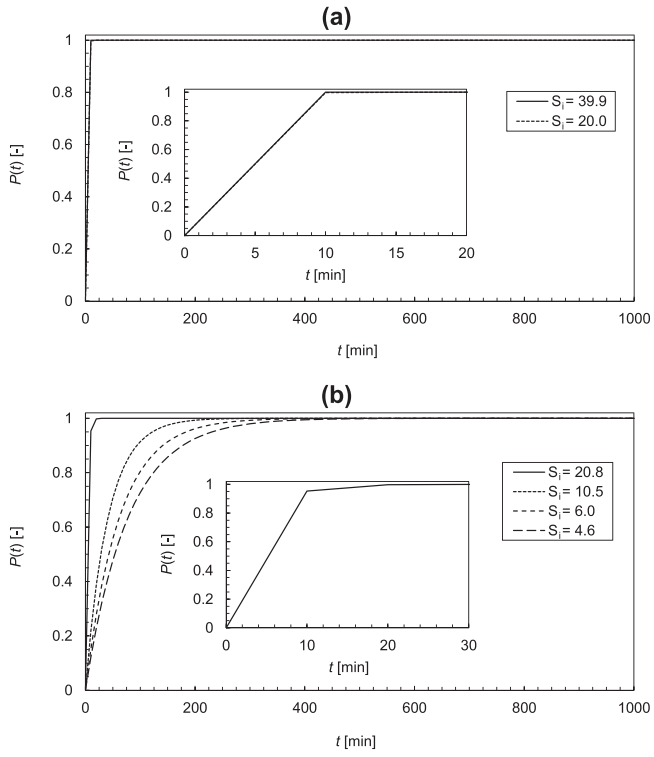

Fig. 4. Probability distribution $P(t)$ [Eq. (A1)] for insulin crystallization assays performed **(a)** in the presence and (the curves are overlapping) **(b)** absence of acetone in the meso OFR-SPC at 20 °C and pH 5.7 at the indicated initial supersaturation values.

ratio (Fig. 3). For the crystallization assays performed in the presence of acetone, an increase in S_i from 20.0 to 39.9 results in an approximately 6-fold decrease in t_{ind}, while in the absence of acetone, an increase in S_i from 10.5 to 20.8 leads to an approximately 12-fold decrease in t_{ind}. These observations indicate that acetone influences the nucleation kinetics of insulin due to a decrease in the solubility concentration value, thus contributing to an increase of the supersaturation ratios at similar insulin concentrations (Table 1). For example, at identical initial supersaturation ratios (conditions A2 and B1, Table 1), t_{ind} is around 2-times shorter in the presence of acetone when compared to the assays carried in the absence of acetone. Moreover, the mean induction time at different initial supersaturation ratios shows a large variation, especially at the lower supersaturation ratios (Fig. 3). These results reflect the stochastic nature of the nucleation process and low nucleation probability at lower initial supersaturation ratios.

At higher supersaturation ratios (conditions A1–A2 and B1–B2, Table 1), the nucleation probability approaches the unit value in a shorter time, which indicates a higher nucleation rate and a shorter induction time [Eq. (A1) and (A2), *see Appendix section*] (Fig. 4). In the presence of acetone, $P(t)$ reaches 1 when $t = 10$ min [$S_i = 20.0$, Fig. 4-(a)], while for the experiments carried out in the absence of acetone $P(t)$ reaches 1 when $t = 20$ min [$S_i = 20.8$, Fig. 4-(b)]. Thus, the probability distributions suggest a faster nucleation event when acetone is present in the crystallization medium due to a solubility decrease. At lower supersaturation values (conditions B3–B4, Table 1), the probability distribution function is well-represented by a characteristic shape representing the stochastic nature of protein nucleation [Fig. 4-(b), Eq. (A1)].

3.1.2. Nucleation rate and number of crystals

The determined nucleation rates [Eq. (A2)] and predicted number of crystals [Eq. (A7)] (*see Appendix section*) in the presence and absence of acetone are displayed in Fig. 5.

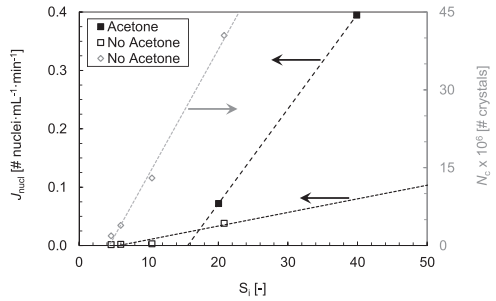

Fig. 5. Overview of the nucleation kinetics of insulin crystallization in the presence and absence of acetone in the meso OFR-SPC at 20 °C and pH 5.7: experimentally measured nucleation rate [Eq. (A2)] and predicted number of crystals [Eq. (A7)] as a function of the initial supersaturation ratio. [Lines are only represented to guide the eye].

An increase in the nucleation rate with the initial supersaturation ratio is observed both in the presence and absence of acetone (Fig. 5). In the presence of acetone, an increase in the supersaturation ratio from 20.0 to 39.9 (conditions A1–A2, Table 1) results in a 5-fold increase in the nucleation rate. In the absence of acetone, an increment in the supersaturation ratio from 10.5 to 20.8 (conditions B1–B2, Table 1) leads to an approximately 12-fold increase in the nucleation rate. Further, at similar supersaturation ratios (conditions A2 and B1, Table 1), the results indicate a nucleation rate about 2-times higher when acetone is added to the crystallization solution (Fig. 5). Regarding the estimated number of crystals, it follows the behavior of the nucleation rate, increasing with the initial supersaturation ratio (Fig. 5). This behavior highlights the major role of acetone in insulin nucleation kinetics and the contribution to higher supersaturation ratios due to the decrease of the solubility concentration.

The results of this study show a faster insulin nucleation event at a high initial supersaturation ratio both in the presence and absence of acetone (Figs. 3–5). According to the CNT [Eq. (A4), *see Appendix section*], there is a strong correlation between homogeneous nucleation rate and supersaturation. The results also highlight the key role of acetone in insulin nucleation kinetics (Figs. 3–5). At similar supersaturation ratios, the nucleation rate is much faster for insulin crystallization assays performed in the presence of acetone (Fig. 5). These findings indicate that the presence of acetone at 15% (v/v) in the crystallization solution accelerates the insulin nucleation process. Acetone at 15% (v/v) has been shown to modify the structure of the water shell around the insulin molecules, thus allowing intermolecular contact (Bergeron et al., 2003; Vekilov, 2007).

3.1.3. Nucleation mechanisms

Using the nucleation rate data from Fig. 5, the linearization expressed by $\ln(J_{nucl}/S_i)$ *versus* $(\ln S_i)^{-2}$ [Eq. (A5), *see Appendix section*] is plotted in Fig. 6, which might suggest the predominant nucleation mechanism (homogeneous or heterogeneous) within the studied supersaturation ratios and the role of acetone in the crystallization medium.

Two regions can be identified: at high supersaturation ratios (conditions A1–A2 and B1–B2, Table 1), an apparent linear decrease suggests a homogenous nucleation regime, while at lower supersaturation ratios (conditions B3–B4, Table 1), a plateau indicates a heterogenous nucleation regime. The parameters A and B [Eq. (A5), *see Appendix section*] can be derived by plotting a straight line through the data points within the homogeneous nucleation regime and neglecting the data points within the heterogeneous region (Table 2).

The parameter B has a similar value when comparing insulin crystallization assays in the presence and absence of acetone, while the parameter A increases around 2.5-times when acetone is added to the crystallization solution (Table 2). Thus, corroborating the shorter

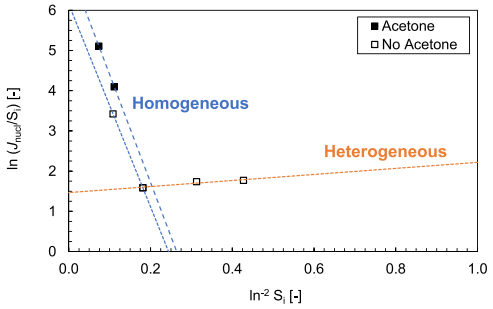

Fig. 6. Plot of $\ln(J_{nucl}/S_i)$ *versus* $(\ln S_i)^{-2}$ to determine the kinetic (*A*) and thermodynamic (B) parameters of the insulin nucleation rate [Eq. (A5), Table 2] and the distinction between homogeneous (high supersaturation ratios) and heterogeneous (low supersaturation ratios) nucleation mechanisms.

Table 2
Overview of the kinetic (*A*) and thermodynamic (B) parameters following the CNT for insulin homogeneous nucleation [Eq. (A5)] in the presence and absence of acetone.

	A [$mL^{-1}{\cdot}s^{-1}$]	B [-]
Acetone	1.2×10^{-3}	26.8
No Acetone	4.7×10^{-4}	25.2

induction times (Fig. 3) and higher nucleation rates (Fig. 5) obtained. The presence of acetone in the crystallization medium at a particular concentration [15% (v/v)] was found to be responsible for the destruction of the water shell around the insulin molecules, thereby exhibiting an impact on the kinetics of molecular attachment (Bergeron et al., 2003; Vekilov, 2007).

The flow conditions in which protein nucleation occurs significantly affect the nucleation kinetics and mechanism (Byington et al., 2017; Castro et al., 2018, 2016; Hammadi et al., 2013; Hekmat, 2015; Hekmat et al., 2007; Judge et al., 1995; Li and Heng, 2021; Penkova et al., 2006; Stroobants et al., 2020; Tait et al., 2009; Yaoi et al., 2004). Both enhancement and suppression of protein nucleation have been reported upon agitated/sheared flow. A non-monotonic dependence of the nucleation rate on the shear rate has been observed, where the nucleation rate increases with the shear rate until a maximum and further increase of the shear rate results in the decrease of the nucleation rate. Ferreira et al. (2022a) optimized the shear rate to reach insulin single large crystals and concluded that shear rates above the optimized value led to crystal breakage. In terms of the underlying mechanisms, enhanced mass transfer and cluster aggregation, and shear-induced molecular alignments might explain the increased nucleation rates (Stroobants et al., 2020), whereas enhanced partial unfolding of protein molecules might justify the suppression of nucleation (Byington et al., 2017). However, this last scenario is more probable at higher temperatures since protein chains experience unfolding at temperatures higher than 37 °C, and all the experiments carried out in the current study were performed at 20 °C (Bouchard et al., 2000; Huus et al., 2005; Nielsen et al., 2001; Wei et al., 2017). During this study, the contact between the bulk solution and the crystallizer glass walls can induce the occurrence of heterogeneous nucleation, which has a lower energetic barrier than homogeneous nucleation (Castro et al., 2018, 2016; Sheridan et al., 2022; Yang et al., 2016). Studies on lysozyme crystallization highlighted that heterogenous nucleation on the glass walls of a vessel predominates over homogeneous nucleation in solution (Roberts et al., 2010; Tsekova, 2009). Insulin heterogeneous nucleation on a bare glass surface has also been reported elsewhere (Nanev et al., 2011b). On the other hand, the oscillatory flow mechanism might promote secondary nucleation through contact and/or shear (Agrawal and Paterson, 2015). The drastic turbidity increase in a short time scale (Fig. 2) is most likely related to the occurrence of secondary nucleation rather than a sudden increase in primary nucleation (Forsyth et al., 2015; Kadam et al., 2011; Kobari et al., 2012; Mullin, 2001).

3.2. Insulin growth rate

3.2.1. Growth rate and final protein concentration

An overview of the crystal growth rates of insulin in the meso-OFR-SPC is given in Fig. 7. Fig. 8 presents the experimentally determined and empirically predicted [Eq. (A8), see Appendix section] growth rates for the crystallization assays carried out in the absence of acetone.

The measured growth rates are within the range 0.044–0.081 μm. min^{-1} (Fig. 7). At similar supersaturation ratios (conditions A2 and B1, and A3 and B2, Table 1), J_{cg} is around 1.3-times higher for the crystallization assays performed in the presence of acetone. This outcome corroborates the results from Table 2, where the estimated kinetic parameter *A* is significantly higher for the assays performed in the presence of acetone, which suggests an acceleration in the kinetics of molecular attachment (Bergeron et al., 2003). Furthermore, the dependence of the growth rate on the initial supersaturation ratio is more pronounced in the presence of acetone. Concerning the final supersaturation ratios in the absence of acetone, Fig. 7 shows a S_f range of 1.1–2.4, which indicates that most of the insulin in solution was consumed during the nucleation events and consequent growth. Therefore, the solubility limit was almost attained.

The empirical growth rate [Eq. (A8), *see Appendix section*] fits well with the experimentally determined growth rate (Fig. 8), where $k_g = 0.05$ μm·min^{-1} and $g = 0.3$. As Eq. (A8) is empirical, thus provides limited information about the crystal growth mechanism. However, if the diffusion step determines the growth rate, usually $g = 1$, while when the surface integration is the limiting step, g has often a higher value (Mullin, 2001).

3.2.2. Crystal size measurements

Representative pictures of insulin crystals formed in the presence (conditions A1–A3, Table 1) and absence (conditions B1–B4, Table 1) of acetone are presented in Fig. 9. The measured insulin mean crystal size as a function of the initial supersaturation ratio is presented in Fig. 10. Lastly, the crystal size distributions (CSD) from the insulin crystallization assays are displayed in Fig. 11 and Table 3.

Insulin crystallizes under a rhombohedral shape both in the presence and absence of acetone (Fig. 9). In the presence of Zn^{2+} ions, insulin monomers assemble to a hexameric form to produce rhombohedral crystallites. In the rhombohedral crystal, the unit cell contains six insulin molecules. The hexamer is assembled from three dimers held together by two or four Zn ions (Nanev et al., 2011a). Hodzhaoglu et al. (2016) verified the formation of well-faceted insulin crystals in the presence of acetone. In the present study, the insulin crystals observed both in the

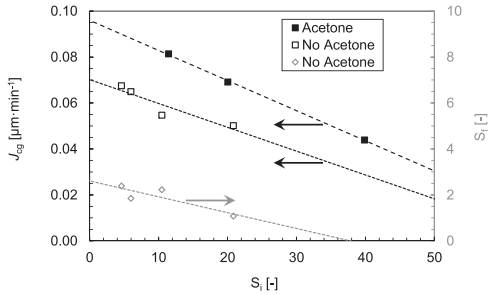

Fig. 7. Overview of the insulin crystallization assays in the presence and absence of acetone in the meso OFR-SPC at 20 °C and pH 5.7: experimentally measured growth rate $[L_c(t)/t]$ and final supersaturation ratio (C_p^f/C_p^{eq}) as a function of the initial supersaturation ratio. [Lines are only represented to guide the eye].

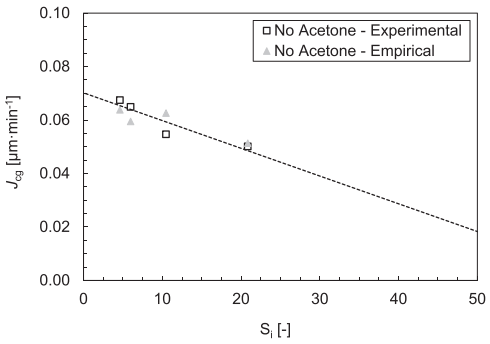

Fig. 8. Comparison between experimentally determined [$L_c(t)/t$] and empirically predicted [Eq. (A8)] growth rates as a function of the initial supersaturation ratio. [Lines are only represented to guide the eye].

presence and absence of acetone show well-defined edges and faces (Fig. 9).

Insulin crystal mean size decreases with the initial supersaturation ratio both in the presence and absence of acetone (Fig. 10). The measured values show a significant variation, especially for the assays carried out in the absence of acetone (Fig. 10). This reflects the dispersion of the insulin CSD [Fig. 11-(b)], while narrower peaks are obtained in the presence of acetone [Fig. 11-(a)]. Moreover, at similar initial supersaturation ratios (conditions A2 and B1, and A3 and B2, Table 1), the mean crystal size is 1.3-times higher in the presence of acetone when compared to the assays in the absence of acetone (Fig. 10).

Insulin CSDs are unimodal with crystal sizes typically ranging between $d_{10} = 2.2$ µm and $d_{90} = 17.3$ µm in the presence of acetone [(Fig. 11-(a), Table 3], and between $d_{10} = 4.3$ µm and $d_{90} = 11.5$ µm in the absence of acetone [Fig. 11-(b), Table 3]. Moreover, the results also indicate a decrease in the insulin crystal size with the initial supersaturation ratio (Fig. 10 and Table 2). These findings agree with the nucleation kinetics (Fig. 5) and growth rates (Fig. 7) data. At high supersaturation ratios, faster nucleation kinetics were obtained and, consequently, a large number of smaller crystals were formed, whereas at lower supersaturation ratios, slower nucleation kinetics were obtained, leading to the formation of fewer but bigger crystals. Therefore, nucleation dominates over growth at higher supersaturation ratios, while growth is the dominating process at lower supersaturation ratios. Concerning the span data results, the CSD is narrower (lower span) in the presence of acetone. Moreover, the span remains similar in the crystallization assays carried out in the presence of acetone regardless of the initial supersaturation. This is also observed in the assays performed in the absence of acetone, expect at the lowest initial supersaturation (Table 3). In addition, the results also show larger crystal sizes in the presence of acetone (Figs. 9–11 and Table 3). For instance, at similar S_i (conditions A2 and B1, Table 1), d_{50} is twice as big for the assays performed in the presence of acetone (9.8 µm) over the experiments carried out in the absence of acetone (5.0 µm). This observation agrees with the estimated crystal growth rates (Fig. 7), where it is verified that at similar S_i insulin crystals grow faster in the presence of acetone. In the presence of acetone, the destruction of the water layer at the hydrophobic moieties on the insulin surface may also lead to enhanced crystal growth. Indeed, studies show that in the presence of acetone, the step kinetic coefficient is around an order of magnitude higher than the one in the absence of acetone (Reviakine et al., 2003). Further, some dispersion in

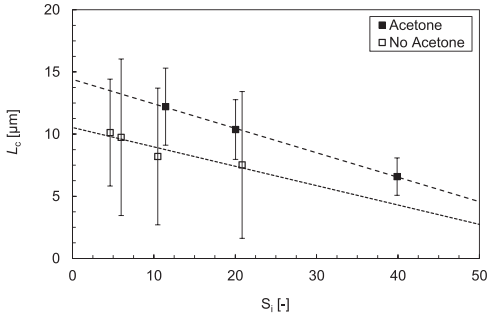

Fig. 10. Crystal size as a function of the initial supersaturation ratio for insulin crystallization assays performed in a meso OFR-SPC at 20 °C and pH 5.7 in the presence and absence of acetone. The error bars are standard deviations from at least three independent experiments. [Lines are only represented to guide the eye].

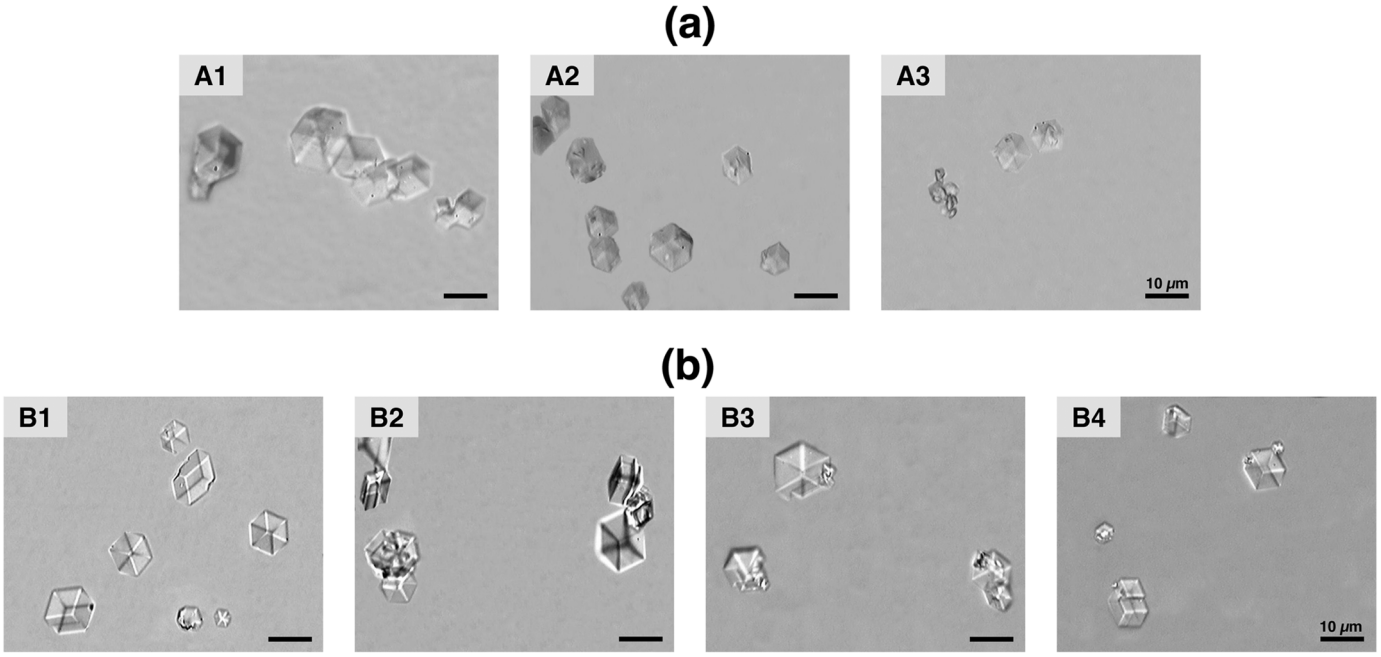

Fig. 9. Optical microscopy images (×10 ×40) of insulin crystals formed at variable initial supersaturation ratio in the meso OFR-SPC at 20 °C and pH 5.7: **(a)** in the presence (conditions A1–A3, Table 1) and **(b)** absence of acetone (conditions B1–B4, Table 1). [The indicated scale bars correspond to a length of 10 µm].

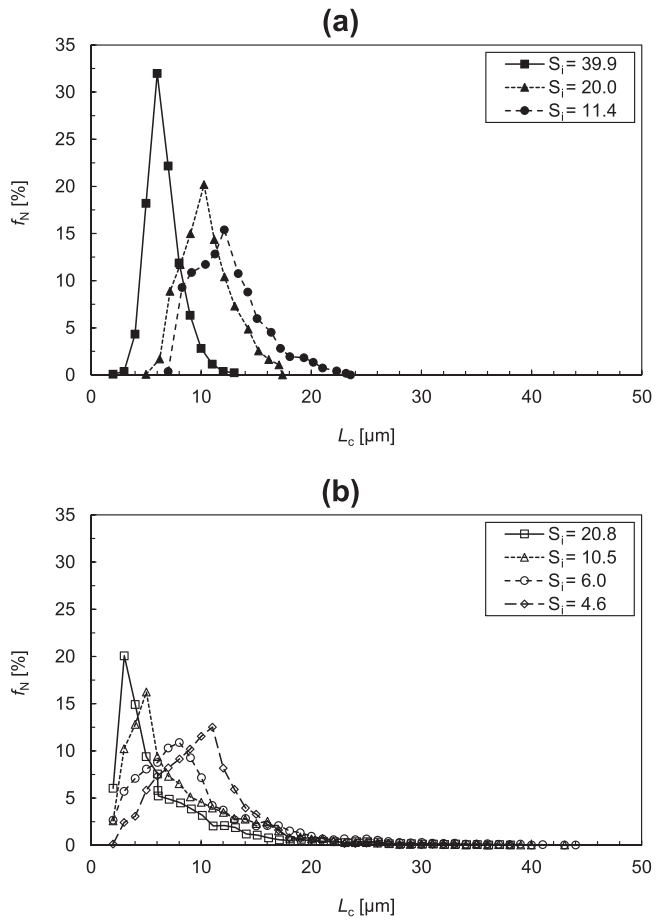

Fig. 11. Insulin crystal size distribution for crystallization assays performed in a meso OFR-SPC at 20 °C and pH 5.7 **(a)** in the presence and **(b)** absence of acetone.

insulin crystal size is observed, especially for the assays carried out in the absence of acetone (Fig. 11 and Table 3). Individual crystals grow under identical conditions (*e.g.*, supersaturation, hydrodynamics, *etc.*) but can grow at different rates (Mullin, 2001). Besides this aspect, heterogeneous nucleation (at the glass walls-solution interface) followed by secondary nucleation may have occurred (*see* section 4.1), which might explain the observed dispersion in the CSD (Fig. 11).

3.3. Crystallization process yield

The estimated crystallization process yields [Eq. (1)] for the insulin crystallization assays carried out in the absence of acetone are given in Table 4.

Most of the insulin in solution was consumed during the crystallization assays as the final insulin concentrations are close to the solubility values (Tables 1 and 4). This consumption is reflected in the high crystallization yields obtained since most of the values are above 60%, except at very low initial supersaturation ratios (conditions B5–B7, Table 1). Moreover, the initial supersaturation ratio has a crucial impact on the crystallization yield. The nucleation rate increases with the initial supersaturation ratio, which leads to the formation of a significant number of crystals (Fig. 5), thus a higher protein consumption in solution.

3.4. Comparison with reported data

Although a direct comparison with the works reported in the literature is not possible due to different crystallization conditions (*e.g.*, precipitant composition, crystallizer type, flow conditions, pH, temperature, *etc.*), it is still relevant to assess the influence of some parameters, such as the presence of acetone, crystallizer type and volume, and flow mechanisms on the nucleation kinetics and growth rate of insulin. An overview of the published studies on the crystallization of insulin at the milliliter scale is provided in Table 5.

3.4.1. Nucleation kinetics

Acetone removes the structured water molecules from the insulin surface (Bergeron et al., 2003; Vekilov, 2007) (*see* section 4.1). Thus, a decrease in insulin solubility would be expected when acetone is added to the crystallization medium, which was observed in this work. Hodzhaoglu et al. (2016) also verified the reduction of the solubility of both human and porcine insulins in the presence of acetone. However, Bergeron et al. (2003) found that porcine insulin solubility rose in the presence of acetone. According to Bergeron and co-workers (Bergeron et al., 2003), when the water structures are destroyed, the crystallization entropy decreases, and the crystallization free energy increases, leading to higher insulin solubility.

Only three studies beyond the present investigation reported insulin

Table 4
Overview of the initial (i) and final (f) insulin concentrations (C_p) and supersaturation levels (S), and process yield (η) [Eq. (1)] for crystallization assays performed in a meso OFR-SPC at 20 °C and pH 5.7 in the absence of acetone.

C_p^i [mg·mL^{-1}]	S_i [-]	C_p^f [mg·mL^{-1}]	S_f [-]	η [%]
2.5 ± 0.04	20.8 ± 0.04	0.1 ± 0.07	1.1 ± 0.06	99.6 ± 0.1
1.2 ± 0.02	10.5 ± 0.2	0.3 ± 0.03	2.2 ± 0.3	87.1 ± 2.9
0.7 ± 0.06	6.0 ± 0.5	0.2 ± 0.04	1.8 ± 0.3	83.0 ± 6.7
0.5 ± 0.08	4.6 ± 0.7	0.3 ± 0.03	2.4 ± 0.3	61.6 ± 6.0
0.3 ± 0.01	2.1 ± 0.08	0.2 ± 0.004	1.8 ± 0.04	25.9 ± 5.3
0.2 ± 0.01	1.9 ± 0.1	0.2 ± 0.01	1.8 ± 0.08	9.2 ± 5.9
0.1 ± 0.003	1.3 ± 0.03	0.1 ± 0.005	1.2 ± 0.04	6.0 ± 5.2

[The errors are standard deviations from at least three independent experiments].

Table 3
Overview of the crystal size measurements at the end of the insulin crystallization assays performed in a meso OFR-SPC at 20 °C and pH 5.7 in the presence and absence of acetone.

	Condition	C_p^i [mg·mL^{-1}]	S_i [-]	$\overline{L}_c$ [μm]	d_{10} [μm]	d_{50} [μm]	d_{90} [μm]	span [-]
Acetone	**A1**	2.5 ± 0.04	39.9 ± 4.8	6.6 ± 1.5	4.3	5.8	8.2	0.7
	A2	1.2 ± 0.02	20.0 ± 2.4	10.4 ± 2.4	7.1	9.8	13.0	0.6
	A3	0.71 ± 0.06	11.4 ± 1.7	12.2 ± 3.1	8.3	11.5	16.4	0.7
No acetone	**B1**	2.5 ± 0.04	20.8 ± 0.04	7.5 ± 5.9	2.2	5.0	12.4	2.0
	B2	1.2 ± 0.02	10.5 ± 0.2	8.2 ± 5.5	2.7	5.9	15.0	2.1
	B3	0.71 ± 0.06	6.0 ± 0.5	9.7 ± 6.3	3.2	7.7	17.3	1.8
	B4	0.55 ± 0.08	4.6 ± 0.7	10.1 ± 4.3	4.8	9.3	14.5	1.0

[d_{10}: 10% of the crystals are smaller than this value, d_{50}: 50% of the crystals are smaller than this value, d_{90}: 90% of the crystals are smaller than this value, and **span** = $(d_{90} - d_{10})/d_{50}$. The errors are standard deviations from at least three independent experiments].

Table 5
Overview of the insulin crystallization conditions and reported outcome variables for the present study and reported works in the literature.

Author (s) & Reference	Protein medium		Precipitant medium				Experimental conditions			Crystallizer specifications		Outcome variables				
	Insulin type & concentration [mg·mL^{-1}]	S [-]	Components & concentrations				T [°C]	pH	t_{exp}	Type & volume	Flow conditions & Operation mode	L_c [μm]	Crystal shape	Crystallization kinetics		η [%]
			Solvent [mM]	Buffer [mM]	Precipitating agent [mM]	Others [%]								J_{nucl} [# nuclei·mL^{-1}·min^{-1}] & t_{ind}	J_{eg} [μm·min^{-1}]	
Present study	**Human recombinant 0.15–2.5**	**1–21 2–40**	**HCl (20)**	**Trisodium citrate (37.5)**	**Zinc chloride (3.8)**	**– Acetone (15)**	**20**	**5.7**	**150 min**	**OFR-SPC $V = 8$ mL**	**Oscillatory flow $f = 1.83$ Hz $x_0 = 5.3$ mm Batch**	**7.5–10.1 6.6–12.2**	**Rhombohedral Rhombohedral**	**0.002–0.04 3–77 min 0.07–0.4 0.3–2 min**	**0.05–0.07* 0.05–0.06# 0.04–0.08***	**6.0–99.6 –**
(Ferreira et al., 2022a)	Human recombinant 0.25–25	8–989	HCl (20)	Trisodium citrate (15.6–46.9)	Zinc chloride (1.6–4.7)	Acetone (3.1–9.4)	5–40	5.7	~ 45–107 min	Rotational rheometer $V \sim 2$ mL	Sheared flow $10^0 \leq \dot{\gamma}$ [s^{-1}] $\leq 10^3$ Batch	–	Rhombohedral	–	–	–
(Link and Heng, 2022)	Human recombinant 0.80–7.02	6–21	Citric acid (100)	HEPES (7) Trisodium citrate (73)	Zinc sulfate Zinc chloride Zinc acetate (1.0–8.2)	–	24	6.0–6.7	~ 90–170 h	Eppendorf tubes $V = 1.5$ mL	Static Batch	–	Rhombohedral	0.0001–0.004 ~ 3–81 h	–	~ 66–88
(Chen et al., 2021)	Human recombinant 1.2–2.4	53–130	HCl (100)	Trisodium citrate (10)	Zinc sulfate (5)	Acetone (15)	10	5.8–6.5	15–30 min	Tubular reactor ($28 \leq \tau$ [min] ≤ 56) $V = 56$ mL	Multiphase (G-L) flow $0.6 \leq Q_L$ [mL·min^{-1}] ≤ 1.2 $0.6 \leq Q_G$ [mL·min^{-1}] ≤ 1.2 Continuous	6.2–10.2	Rhombohedral	–	0.2–0.4* 0.3–0.4#	~ 85–98
(Hirata et al., 2012)	Porcine insulin 2.0	3–182	H_2O HCl (4)	Sodium bicarbonate (50)	Zinc chloride (0.4)	CO_2 (atm)	15	6.3–7.34	22–103 h	Cylindrical stainless-steel vessel $V = 340$ mL	Agitation (impeller: 30 rpm) and pressure Batch	9.3–23.0	Rhombohedral	–	0.002–0.01* 0.005–0.01#	–
(Parambil et al., 2011)	Human recombinant 2.5	–	H_2O	Trisodium citrate (480)	Zinc sulfate (31)	Acetone (10)	10	6.0	48 h	Glass capillaries $d_c = 2$ mm	Oscillatory flow $0.25 \leq \dot{\gamma}$ [s^{-1}] ≤ 0.65 $f = 0.02$ Hz $6 \leq x_0$ [mm] ≤ 16 Batch	–	Rhombohedral	–	–	~ 23–50
(Hirata et al., 2010)	Porcine insulin 1.8	6–13	H_2O HCl (4)	Sodium bicarbonate (50)	Zinc chloride (0.4)	CO_2 (atm)	5 15	6.35–6.5	19 h	Cylindrical stainless-steel vessel $V = 340$ mL	Agitation (stirrer: 120 rpm) and pressure Batch	7.6–10.6	Rhombohedral	–	0.007–0.009* 0.01#	81–83
									19–40 h		Agitation (impeller: 65 rpm) and pressure Batch	14.8–19.6			0.008–0.01* 0.01#	86–92

(*continued on next page*)

Table 5 (*continued*)

Author (s) & Reference	Protein medium		Precipitant medium				Experimental conditions			Crystallizer specifications		Outcome variables			
	Insulin type & concentration [mg·mL^{-1}]	S [-]	Components & concentrations				T [°C]	pH	t_{exp}	Type & volume	Flow conditions & Operation mode	L_c [μm]	Crystal shape	Crystallization kinetics	η [%]
			Solvent [mM]	Buffer [mM]	Precipitating agent [mM]	Others [%]								J_{nucl} [# nuclei·mL^{-1}·min^{-1}] & t_{ind}	J_{cg} [μm·min^{-1}]	
(Penkova et al., 2004)	Porcine insulin 2.0	1.7–2.3[§]	HCl (1)	Citrate buffer (50)	Zinc chloride (5)	Acetone (15)	5–23	6.98	~ 2 days	Glass capillaries $V \sim 2$ mL	Static Batch	~ 1000	Rhombohedral	0.002–0.009[¶] –	~ 0.3*	–
(Bernardo et al., 2004)	Porcine insulin 1.2–4.4	2–6 (T = 25 °C, pH = 5.5) 10–24 (T = 25 °C, pH = 6.59)	H_2O	Sodium acetate (100)	Sodium chloride (1198)	Acetic acid (100)	15 25 35	3.23 5.5 6.59	> 2 days	Quartz cuvettes $V = 2$ mL	Batch	–	Rhombohedral	0.01–0.1 4–52 min (T = 25 °C, pH = 5.5) 0.02–0.3 1–21 min (T = 25 °C, pH = 6.59)	–	–

[**Notes**: [§] The authors defined the thermodynamic supersaturation as $\Delta\mu$ ($\Delta\mu = k_B T\sigma$), where k_B is the Boltzmann's constant, T the absolute temperature, and σ depends on the solute activity [$\sigma = \ln(2/C_p^{eq})$]. [¶] Calculated based on the induction time (t_{ind}) and experimental volume (V): $1/(t_{ind}V)$. * Calculated based on the experimentally measured crystal size (L_c) and duration of the crystallization assay (t_{exp}): L_c/t_{exp}. [#] Calculated based on the experimentally measured final (C_p^f) and equilibrium (C_p^{eq}) protein concentrations: $k_g\left(C_p^f/C_p^{eq}\right)^g$. [¶] Calculated based on the experimentally measured number of nucleus and respective time interval].

nucleation kinetics data. When comparing the induction times and nucleation rates in Table 5, it is possible to highlight the impact of the supersaturation level, the presence of acetone, pH, and flow conditions on the insulin nucleation kinetics. Bernardo et al. (2004) found similar nucleation kinetics data compared to the results obtained herein in the presence of acetone, crystallizing insulin at similar supersaturation ratios but different solution composition (in the absence of acetone). In the work reported by Penkova et al. (2004), nucleation rates were similar to the values herein obtained in the absence of acetone at the lowest supersaturation ratios. However, the authors used acetone and worked at higher pH. It has been shown that acetone accelerates insulin nucleation kinetics (Bergeron et al., 2003) (*see* section 4.1). Shorter onset of insulin nucleation was also verified in a more basic medium (Link and Heng, 2022). In contrast, much slower nucleation kinetics were found by Link and Heng (2022). On the one hand, the authors performed crystallization assays in the absence of acetone. On the other hand, insulin was crystallized under static conditions, while in the current study crystallization experiments were carried out under oscillatory flow mixing. These hydrodynamic conditions may induce heterogeneous nucleation and further secondary nucleation (*see* section 4.1), thus explaining the higher nucleation rates obtained.

3.4.2. Nucleation mechanisms

The insulin nucleation mechanism in the meso OFR-SPC is mostly homogenous at high supersaturation ratios (conditions A1–A2 and B1–B2, Table 1), while heterogeneous nucleation is preponderant (Fig. 6) at low supersaturation ratios (conditions B3–B4). This nucleation behavior was also observed byLink and Heng (2022) and Bernardo et al. (2004), where the nucleation data reveal a homogeneous regime at high supersaturation ratios (7.3–15.9 in (Link and Heng, 2022), and 5.6–10.2 in (Bernardo et al., 2004)) and a heterogeneous regime at low supersaturation ratios (5.6–5.7 in (Link and Heng, 2022), and 1.9–2.6 in (Bernardo et al., 2004)). Contrary to the crystallization assays reported in the literature and carried out under static conditions, insulin crystallization in the current work was studied under an oscillatory flow mechanism. For this reason, heterogeneous nucleation may occur at the crystallizer glass walls-solution interface (Sheridan et al., 2022; Yang et al., 2016). Moreover, collisions of primary crystals with other crystals and/or crystallizer walls may induce secondary nucleation through contact and/or shear (Castro et al., 2018, 2016).

3.4.3. Crystal growth rates

Insulin growth rate data are scare in the literature, thus most of the growth rate values highlighted in Table 5 were estimated based on two different methodologies: crystal size and duration of the crystallization experiments [$L_c(t)/t$], and final supersaturation values through an empirical power law [$k_g(S_f)^g$] (*see* Section 2.2). In general, growth rates are faster when acetone is present in the crystallization medium (Table 5). This behavior is in accordance with the data reported by Bergeron et al. (2003) and with the current results, where higher J_{cg} were obtained in the presence of acetone when compared to the crystallization assays in the absence of acetone (Fig. 7). This outcome is explained by the impact in the supersaturation due to a decreased solubility concentration. For instance, Chen et al. (2021) found higher insulin growth rates when compared to the current study, but the authors used much higher supersaturation ratios and worked under continuous mode. When comparing the estimated growth parameters following a similar methodology [Eq. (A8), *see Appendix section*], it is possible to notice that the values of the parameter g are similar for the mentioned works (Table 6). Furthermore, k_g is much higher for the crystallization experiments performed in the presence of acetone [present study and Chen et al. (2021)].

3.4.4. Crystal shape and size measurements

Insulin crystals formed in this study and reported in literature

Table 6
Overview of the growth constant (k_g) and exponent (g) values predicted by the empirical crystal growth model [Eq. (A8)] for the present study and reported works in the literature.

Author (s) & Reference	k_g [μm·min^{-1}]	g [-]
Present study	0.05	0.3
(Chen et al., 2021)	0.24	0.2
(Hirata et al., 2012)	0.002	0.5
(Hirata et al., 2010)	0.008	0.1

present a rhombohedral shape for all the studied experimental conditions (Table 5). In most of the reported works, insulin crystallization was carried out in the presence of zinc ions. Insulin crystallizes under a rhombohedral shape in the presence of Zn^{2+} ions, where insulin monomers assemble to a hexameric form (Nanev et al., 2011a). Nevertheless, Bernardo et al. (2004) reported the formation of rhombohedral insulin crystals in the absence of zinc ions.

Insulin crystals range within 6–23 μm in the published works, except in the study from Penkova et al. (2004), where crystals size reaches values up to 1000 μm, but crystallization assays were extended to 2 days. According to Basu et al. (2004), insulin crystals with a size of up to 20 μm can be used in long-acting injectable formulations for prolonged glucose control.

3.4.5. *Crystallization yield*

Reported crystallization yields in Table 5 are usually higher than 60%, except in the study from Parambil et al. (2011), where crystallization yields are within the range of 23–50%. Herein, estimated crystallization yields are above 60%, except at the lowest initial supersaturation ratios (conditions B5–B7, Table 1). It should be noted that most of the batch crystallization experiments mentioned in Table 5 have much longer operating times (several hours to days) than the present work (150 min). Chen et al. (2021) performed crystallization assays with shorter operation times (continuous mode), but much higher supersaturation rates were employed.

4. Conclusion

This work presents a unique platform based on smoothed-oscillatory flow to crystallize insulin, which contributes to the development of a standardized methodology for simultaneous investigation and *in-line* monitoring of protein crystallization assays at the meso scale. This interdisciplinary approach allows the experimental quantification of nucleation kinetics and growth rates data by following the *Classical Nucleation Theory*. Thus, contributing to fill the current gap in the literature, where both nucleation and growth kinetics data are lacking regardless of the crystallization scale. The main outcomes include: (i) the production and quantification of rhombohedral insulin crystals (crystal shape and number, CSD, and crystallization yield) and (ii) the estimation of insulin crystallization kinetics (induction time, nucleation and growth rates, and final insulin concentration) both in the presence and absence of acetone as co-solvent for a wide range of initial supersaturation ratios. Despite the short experimental time (150 min) compared to other studies reported in the literature, the insulin crystallization outcomes are within the literature ranges. However, additional crystallization conditions should be tested in a future study to completely characterize insulin crystallization kinetics in an oscillatory-based reactor, with a special focus on growth kinetics.

The experimental results reveal short induction times, narrow CSD, and high crystallization process yields, where acetone plays a major role in the insulin nucleation kinetics due to the impact on the solubility limit and, consequently, on the supersaturation ratio. Therefore, smoothed-oscillatory flow experimentation constitutes a promising technology for controlling protein nucleation. This behaviour has been highlighted along the current study for insulin and before with lysozyme through optimized oscillatory conditions (mixing intensity) (Castro et al., 2018) and seeding (Castro et al., 2022a). These aspects open new perspectives for crystallizing other macromolecules, or even the transition to continuous crystallization manufacturing and/or crystallization process scalability. Moreover, there has been an increasing focus on long-acting crystalline drug formulations to replace frequent subcutaneous injections, the primary insulin administration route (Norrman and Schluckebier, 2007). The slow dissolution rate of protein crystals allows sustainable drug release, where narrow CSD and shape uniformity are required (Brange, 1987). The results presented in this study fulfil these two requisites. Additionally, insulin crystals with a size up to 20 μm can be used in long-acting injectable drug formulations (Basu et al., 2004), which encloses the obtained crystal size range.

CRediT authorship contribution statement

The manuscript was written through the contributions of all authors. All authors have approved the final version of the manuscript. **Joana Ferreira**: Conceptualization, Methodology, Investigation, Writing – original draft. **Sofia Araújo**: Methodology, Investigation. **António Ferreira**: Methodology, Writing – review & editing. **José Teixeira**: Funding acquisition, Supervision. **João Moreira de Campos**: Funding acquisition, Supervision, Writing – review & editing. **Fernando Rocha**: Funding acquisition, Supervision, Writing – review & editing. **Filipa Castro**: Conceptualization, Methodology, Investigation, Writing – original draft.

Declaration of Competing Interest

The authors declare that they have no known competing financial interests or personal relationships that could have appeared to influence the work reported in this paper.

Acknowledgements

J. F. acknowledges funding from CEFT under FCT/MCTES (PIDDAC) through a postdoctoral scholarship. F. C. acknowledges FCT for the CEEC Individual Contract (https://doi.org/10.54499/2022.06818.CEECIND/CP1718/CT0022). This work was financially supported by: HealthyWaters (NORTE-01-0145-FEDER-000069), supported by Norte Portugal Regional Operational Programme (NORTE 2020), under the PORTUGAL 2020 Partnership Agreement, through the European Regional Development Fund (ERDF); and LA/P/0045/2020 (ALiCE), UIDB/00532/2020 and UIDP/00532/2020 (CEFT), UIDB/00511/2020 and UIDP/00511/2020 (LEPABE), and UIDB/04469/2020 (CEB) and LA/P/0029/2020 (LABBELS), funded by national funds through FCT/MCTES (PIDDAC).

Appendix – Theory

A1. Nucleation kinetics

Nucleation (*i.e.,* the appearance of a nucleus) has a stochastic nature, which is reflected by induction time variations at identical conditions. A probability distribution function describes the probability of detecting nuclei as a function of time in a certain volume and assuming a constant supersaturation. The solution volume can be divided into a large number of small independent volumes. In such small volumes, a nucleation event can

be assumed to be stochastic, thus modeled by a Poisson distribution (Jiang and ter Horst, 2011; Krishnan, 2006; Nappo et al., 2018; Rossi et al., 2015). At a constant supersaturation level, the theoretical probability $P(t)$ [-] that at least one stable nucleus forms in a volume (V [m^3]) during a certain time (t [s]) is given by Eq. (A1) (Jiang and ter Horst, 2011).

$$P(t) = 1 - \exp(-J_{nucl}\, V\, t), \tag{A1}$$

where J_{nucl} [# of nuclei·m^{-3}·s^{-1}] is the nucleation rate (number of nuclei per unit volume and per unit time). Following the single nucleation mechanism (Brandel and ter Horst, 2015; Jiang and ter Horst, 2011; Shiau, 2022), as soon as this probability reaches values close to the unit [$P(t)\rightarrow 1$], the time interval corresponds to the induction time (t_{ind}) and Eq. (A2) is derived.

$$1 = J_{nucl}\, V\, t_{ind}. \tag{A2}$$

Lastly, by assuming homogeneous nucleation events, t_{ind} can be considered to be inversely proportional to the J_{nucl} as defined by Eq. (A3) (Mullin, 2001).

$$t_{ind} = \frac{1}{J_{nucl}\, V}. \tag{A3}$$

The induction time is the period that elapses between the achievement of supersaturation and the appearance of crystals. The latter is made up of several parts: (1) relaxation time (*i.e.,* the time required for the system to achieve a quasi-steady-state distribution of molecular clusters), (2) time required for the formation of a stable nucleus, and (3) time needed for the nucleus to grow to a detectable size (Mullin, 2001).

According to the *Classical Nucleation Theory* (CNT), the homogeneous nucleation rate (J_{nucl} [# of nuclei·m^{-3}·s^{-1}]) as a function of the supersaturation level (S [-]) is given by Eq. (A4) (Brandel and ter Horst, 2015; Mullin, 2001).

$$J_{nucl}(\mathrm{S}) = A\ \mathrm{S} \exp\left[-\frac{\mathrm{B}}{(\ln \mathrm{S})^2}\right], \tag{A4}$$

where A [# of nuclei·m^{-3}·s^{-1}] and B [-] are kinetic and thermodynamic parameters, respectively. The parameter A describes the molecular attachment kinetics, while the parameter B is related to the nucleation barrier that must be overcome. By linearizing and rewriting Eq. (A4), Eq. (A5) can be derived.

$$\ln\left(\frac{J_{nucl}}{\mathrm{S}}\right) = \ln A - \frac{\mathrm{B}}{(\ln \mathrm{S})^2}, \tag{A5}$$

by plotting $\ln(J_{nucl}/\mathrm{S})$ *versus* $(\ln \mathrm{S})^{-2}$, the parameters A (from the line's intercept) and B (from the line's slope) can be derived.

A2. Growth rate

The amount of protein in a solution that is transported from the bulk phase to the crystal at a certain time t [s] can be obtained by Eq. (A6) (Dombrowski et al., 2010; Ferreira et al., 2020; Kwon et al., 2014).

$$V\underbrace{\Delta C_p(t)}_{C_p^i - C_p^f} = \rho_c \overbrace{\Delta V_c(t)}^{k_v\, L_c(t)^3}\, N_c(t), \tag{A6}$$

where $\Delta C_p(t)$ [$kg{\cdot}m^{-3}$] and $\Delta V_c(t)$ [m^3] are the changes in protein concentration (C_p^i [$kg{\cdot}m^{-3}$] and C_p^f [$kg{\cdot}m^{-3}$] are the initial and final protein concentrations, respectively) and crystal volume in the time interval Δt [s], respectively. ρ_c [$kg{\cdot}m^{-3}$] is the crystal density (specific protein density, 1.09 $g{\cdot}cm^{-3}$ for insulin (Crowfoot, 1938)), k_v [-] the volumetric shape factor (corresponding to 1 for rhombohedral crystals), $L_c(t)$ [m] the crystal size at time t, and $N_c(t)$ [-] the number of crystals at time t. By algebraic manipulation of Eq. (A6), the variable $N_c(t)$ can be isolated in the first term of Eq. (A7) (Li et al., 2017; Wang et al., 2008).

$$N_c(t) = \frac{V\left(C_p^i - C_p^f\right)}{\rho_c\, k_v\, L_c(t)^3}. \tag{A7}$$

The crystal growth rate at time t [$J_{cg}(t)$] [$m{\cdot}s^{-1}$] can be estimated by an empirical power law using [Eq. (A8)] (Hirata et al., 2012; Mullin, 2001; Shi et al., 2005; Wang et al., 2008).

$$J_{cg}(t) = k_g \left[\frac{C_p(t)}{C_p^{eq}}\right]^g = k_g[\mathrm{S}(t)]^g, \tag{A8}$$

where k_g [$m{\cdot}s^{-1}$] and g [-] are the growth constant and exponent, which are determined by minimizing the sum of quadratic errors between the empirical data [Eq. (A8)] and experimentally obtained growth rates [$L_c(t)/t$]. C_p^{eq} [$kg{\cdot}m^{-3}$] is the protein equilibrium concentration (solubility concentration), and $\mathrm{S}(t)$ [-] the supersaturation at time t [s].

References

Agrawal, S.G., Paterson, A.H.J., 2015. Secondary nucleation: mechanisms and models. Chem. Eng. Commun. 202, 698–706. https://doi.org/10.1080/00986445.2014.969369.

Agyei, D., Ahmed, I., Akram, Z., M. N. Iqbal, H., K. Danquah, M., 2017. Protein and peptide biopharmaceuticals: an overview. Protein Pept. Lett. 24, 94–101. https://doi.org/10.2174/0929866523666161222150444.

Almeida, F., Rocha, F., Teixeira, J.A., Ferreira, A., 2022. The influence of electrolytes in aqueous solutions on gas-liquid mass transfer in an oscillatory flow reactor. Chem. Eng. Sci. 263 https://doi.org/10.1016/j.ces.2022.118048.

Araújo, S.M., 2022. Towards protein crystallization as a tool for bio-separation: study of insulin crystallization in a meso oscillatory flow reactor. Faculty of Engineering of the University of Porto, Porto, Portugal.

Basu, S.K., Govardhan, C.P., Jung, C.W., Margolin, A.L., 2004. Protein crystals for the delivery of biopharmaceuticals. Expert Opin. Biol. Ther. 4, 301–317.

Bergeron, L., Filobelo, L.F., Galkin, O., Vekilov, P.G., 2003. Thermodynamics of the hydrophobicity in crystallization of insulin. Biophys. J. 85, 3935–3942. https://doi.org/10.1016/S0006-3495(03)74807-3.

Bernardo, A., Calmanovici, C.E., Alves Miranda, E., 2004. Induction time as an instrument to enhance comprehension of protein crystallization. Cryst. Growth Des. 4, 799–805. https://doi.org/10.1021/cg034170.

Bouchard, M., Zurdo, J., Nettleton, E.J., Dobson, C.M., Robinson, C.V., 2000. Formation of insulin amyloid fibrils followed by FTIR simultaneously with CD and electron microscopy. Protein Sci. 9, 1960–1967. https://doi.org/10.1110/ps.9.10.1960.

Brandel, C., ter Horst, J.H., 2015. Measuring induction times and crystal nucleation rates. Faraday Discuss. 179, 199–214. https://doi.org/10.1039/C4FD00230J.

Brange, J., 1987. Galenics of Insulin: The Physico-chemical and Pharmaceutical Aspects of Insulin and Insulin Preparations, 1st edition. Springer-Verlag, Berlin Heidelberg, Berlin, Germany.

Byington, M.C., Safari, M.S., Conrad, J.C., Vekilov, P.G., 2017. Shear flow suppresses the volume of the nucleation precursor clusters in lysozyme solutions. J. Cryst. Growth 468, 493–501. https://doi.org/10.1016/J.JCRYSGRO.2016.12.080.

Castro, F., Cunha, I., Ferreira, A., Teixeira, J.A., Rocha, F., 2022a. Towards an enhanced control of protein crystallization: Seeded batch lysozyme crystallization in a meso oscillatory flow reactor. Chem. Eng. Res. Des. 178, 575–582.

Castro, F., da Silva, N.R., Silvério, S.C., Ballesteros, L.F., Teixeira, J.A., 2022b. Unit operations for extraction and purification of biological products. In: Sirohi, R., Pandey, A., Taherzadeh, M.J., Larroche, C. (Eds.), Current Developments in Biotechnology & Bioengineering. Elsevier, pp. 455–495. https://doi.org/10.1016/B978-0-323-91167-2.00005-8.

Castro, F., Ferreira, A., Teixeira, J.A., Rocha, F., 2018. Influence of mixing intensity on lysozyme crystallization in a meso oscillatory flow reactor. Cryst. Growth Des. 18, 5940–5946. https://doi.org/10.1021/acs.cgd.8b00721.

Castro, F., Ferreira, A., Teixeira, J.A., Rocha, F., 2016. Protein crystallization as a process step in a novel meso oscillatory flow reactor: study of lysozyme phase behavior. Cryst. Growth Des. 16, 3748–3755. https://doi.org/10.1021/acs.cgd.6b00262.

Chen, J., Sarma, B., Evans, J.M.B., Myerson, A.S., 2011. Pharmaceutical crystallization. Cryst. Growth Des. 11, 2662–2679.

Chen, R., Weng, J., Chow, S.F., Lakerveld, R., 2021. Integrated continuous crystallization and spray drying of insulin for pulmonary drug delivery. Cryst. Growth Des. 21, 501–511. https://doi.org/10.1021/acs.cgd.0c01312.

Crowfoot, D., 1938. The crystal structure of insulin. I. The investigation of air-dried insulin crystals. Proc. R. Soc. A: Math. Phys. Eng. Sci. 164, 580–602.

Cruz, P., Rocha, F., Ferreira, A., 2018. Determination of the critical mixing intensity for secondary nucleation of paracetamol in an oscillatory flow crystallizer. CrystEngComm 20, 829–836. https://doi.org/10.1039/C7CE01940H.

Cruz, P., Rocha, F., Ferreira, A., 2016. Effect of operating conditions on batch and continuous paracetamol crystallization in an oscillatory flow mesoreactor. CrystEngComm 18, 9113–9121. https://doi.org/10.1039/C6CE01648K.

Dombrowski, R.D., Litster, J.D., Wagner, N.J., He, Y., 2010. Modeling the crystallization of proteins and small organic molecules in nanoliter drops. AIChE J. 56, 79–91. https://doi.org/10.1002/aic.12001.

dos Santos, R., Carvalho, A.L., Roque, A.C.A., 2017. Renaissance of protein crystallization and precipitation in biopharmaceuticals purification. Biotechnol. Adv. 35, 41–50. https://doi.org/10.1016/j.biotechadv.2016.11.005.

Faria, N., Pons, M.N., Feyo de Azevedo, S., Rocha, F.A., Vivier, H., 2003. Quantification of the morphology of sucrose crystals by image analysis. Powder Technol. 133, 54–67. https://doi.org/10.1016/S0032-5910(03)00078-0.

Ferreira, A., Rocha, F., Teixeira, J.A., Castro, F., 2019. Modular oscillatory flow plate reactor. EP 3439773 A1.

Ferreira, A., Rocha, F., Teixeira, J.A., Vicente, A., 2016a. Apparatus for mixing improvement based on oscillatory flow reactors provided with smooth periodic constrictions. US 2016/0250615 A1.

Ferreira, A., Rocha, F., Teixeira, J.A., Vicente, A., 2016b. Apparatus for mixing based on oscillatory flow reactors provided with smooth periodic constrictions. EP 3057694 A1.

Ferreira, A., Teixeira, J.A., Rocha, F., 2015. O2 mass transfer in an oscillatory flow reactor provided with smooth periodic constrictions. Individual characterization of kL and a. Chem. Eng. J. 262, 499–508. https://doi.org/10.1016/j.cej.2014.09.125.

Ferreira, J., Carneiro, J., de Campos, J.M., 2022a. Shear-induced crystallization and rheological analysis of a therapeutic protein. Cryst. Growth Des. 22, 6440–6455. https://doi.org/10.1021/acs.cgd.2c00557.

Ferreira, J., Castro, F., Kuhn, S., Rocha, F., 2020. Controlled protein crystal nucleation in microreactors: the effect of the droplet volume versus high supersaturation ratios. CrystEngComm 22, 4692–4701. https://doi.org/10.1039/d0ce00517g.

Ferreira, J., Zsuzsa, S., Castro, F., Rocha, F., Kuhn, S., 2022b. Insulin crystallization: the route from hanging-drop vapour diffusion to controlled crystallization in droplet microfluidics. J. Cryst. Growth 582, 1–12. https://doi.org/10.1016/j.jcrysgro.2022.126516.

Forsyth, Carol, Mulheran, P.A., Forsyth, Claire, Haw, M.D., Burns, I.S., Sefcik, J., 2015. Influence of controlled fluid shear on nucleation rates in glycine aqueous solutions. Cryst. Growth Des. 15, 94–102. https://doi.org/10.1021/cg5008878.

García-Ruiz, J.M., 2003. Nucleation of protein crystals. J. Struct. Biol. 142, 22–31. https://doi.org/10.1016/S1047-8477(03)00035-2.

Gonçalves, A.L., Almeida, F., Rocha, F.A., Ferreira, A., 2021. Improving CO_2 mass transfer in microalgal cultures using an oscillatory flow reactor with smooth periodic constrictions. J. Environ. Chem. Eng. 9, 1–12. https://doi.org/10.1016/j.jece.2021.106505.

Graça, C.A.L., Lima, R.B., Pereira, M.F.R., Silva, A.M.T., Ferreira, A., 2020. Intensification of the ozone-water mass transfer in an oscillatory flow reactor with innovative design of periodic constrictions: optimization and application in ozonation water treatment. Chem. Eng. J. 389, 1–8. https://doi.org/10.1016/j.cej.2020.124412.

Hammadi, Z., Candoni, N., Grossier, R., Ildefonso, M., Morin, R., Veesler, S., 2013. Small-volume nucleation. C R Phys. 14, 192–198. https://doi.org/10.1016/j.crhy.2012.12.004.

Hekmat, D., 2015. Large-scale crystallization of proteins for purification and formulation. Bioprocess Biosyst. Eng. 38, 1209–1231. https://doi.org/10.1007/s00449-015-1374-y.

Hekmat, D., Hebel, D., Schmid, H., Weuster-Botz, D., 2007. Crystallization of lysozyme: from vapor diffusion experiments to batch crystallization in agitated mL-scale vessels. Process Biochem. 42, 1649–1654. https://doi.org/10.1016/j.procbio.2007.10.001.

Hirata, G.A.M., Bernardo, A., Miranda, E.A., 2012. Determination of crystal growth rate for porcine insulin crystallization with CO_2 as a volatile acidifying agent. Chem. Eng. Process.: Process.Intensif. 56, 29–33. https://doi.org/10.1016/j.cep.2012.03.001.

Hirata, G.A.M., Bernardo, A., Miranda, E.A., 2010. Crystallization of porcine insulin with carbon dioxide as acidifying agent. Powder Technol. 197, 54–57. https://doi.org/10.1016/j.powtec.2009.08.017.

Hodzhaoglu, F.V., Conejero-Muriel, M., Dimitrov, I.L., Gavira, J.A., 2016. Optimization of the classical method for nucleation and growth of rhombohedral insulin crystals by pH titration and screening. Bulg. Chem. Commun. 48, 29–37.

Huus, K., Havelund, S., Olsen, H.B., Van De Weert, M., Frokjaer, S., 2005. Thermal dissociation and unfolding of insulin. Biochemistry 44, 11171–11177. https://doi.org/10.1021/bi0507940.

ImageJ [WWW Document], 2019. ImageJ. URL ⟨https://imagej.net/ImageJ⟩ (accessed 4.1.23).

Jiang, S., ter Horst, J.H., 2011. Crystal nucleation rates from probability distributions of induction times. Cryst. Growth Des. 11, 256–261. https://doi.org/10.1021/cg101213q.

Judge, R.A., Johns, M.R., White, E.T., 1995. Protein purification by bulk crystallization: the recovery of ovalbumin. Biotechnol. Bioeng. 48, 316–323.

Kadam, S.S., Kramer, H.J.M., ter Horst, J.H., 2011. Combination of a single primary nucleation event and secondary nucleation in crystallization processes. Cryst. Growth Des. 11, 1271–1277. https://doi.org/10.1021/cg101504c.

Kobari, M., Kubota, N., Hirasawa, I., 2012. Secondary nucleation-mediated effects of stirrer speed and growth rate on induction time for unseeded solution. CrystEngComm 14, 5255–5261. https://doi.org/10.1039/C2CE25248A.

Krishnan, V., 2006. Probability and Random Processes. John Wiley & Sons.

Kwon, J.S.L., Nayhouse, M., Christofides, P.D., Orkoulas, G., 2014. Protein crystal shape and size control in batch crystallization: comparing model predictive control with conventional operating policies. Ind. Eng. Chem. Res 53, 5002–5014. https://doi.org/10.1021/ie400584g.

Li, F., Lakerveld, R., 2017. Influence of alternating electric fields on protein crystallization in microfluidic devices with patterned electrodes in a parallel-plate configuration. Cryst. Growth Des. 17, 3062–3070. https://doi.org/10.1021/acs.cgd.6b01846.

Li, H., Kawajiri, Y., Grover, M.A., Rousseau, R.W., 2017. Modeling of nucleation and growth kinetics for unseeded batch cooling crystallization. Ind. Eng. Chem. Res 56, 4060–4073. https://doi.org/10.1021/acs.iecr.6b04914.

Li, X., Heng, J.Y.Y., 2021. The critical role of agitation in moving from preliminary screening results to reproducible batch protein crystallisation. Chem. Eng. Res. Des. 173, 81–88. https://doi.org/10.1016/j.cherd.2021.06.012.

Link, F.J., Heng, J.Y.Y., 2022. Unraveling the impact of pH on the crystallization of pharmaceutical proteins: a case study of human insulin. Cryst. Growth Des. 22, 3024–3033. https://doi.org/10.1021/acs.cgd.1c01463.

Link, F.J., Heng, J.Y.Y., 2021. Enhancing the crystallisation of insulin using amino acids as soft-templates to control nucleation. CrystEngComm 23, 3951–3960. https://doi.org/10.1039/d1ce00026h.

Mathew Thomas, K., Nyande, B.W., Lakerveld, R., 2022. Design and characterization of Kenics static mixer crystallizers. Chem. Eng. Res. Des. 179, 549–563. https://doi.org/10.1016/j.cherd.2022.01.025.

McPherson, A., Gavira, J.A., 2014. Introduction to protein crystallization. Acta Crystallogr F. Struct. Biol. Commun. 70, 2–20. https://doi.org/10.1107/S2053230×13033141.

Mühlig, P., Klupsch, T., Schell, U., Hilgenfeld, R., 2001. Observation of the early stage of insulin crystallization by confocal laser scanning microscopy. J. Cryst. Growth 232, 93–101. https://doi.org/10.1016/S0022-0248(01)01070-3.

Mullin, J.W., 2001. Crystallization, 4th Edition. ed. Oxford, United Kingdom. https://doi.org/10.1002/0471238961.0318251918152119.a01.pub3.

Nanev, C.N., 2020. Advancements (and challenges) in the study of protein crystal nucleation and growth; thermodynamic and kinetic explanations and comparison with small-molecule crystallization. Prog. Cryst. Growth Charact. Mater. 66, 1–23. https://doi.org/10.1016/j.pcrysgrow.2020.100484.

Nanev, C.N., 2013. Kinetics and intimate mechanism of protein crystal nucleation. Prog. Cryst. Growth Charact. Mater. 59, 133–169. https://doi.org/10.1016/j.pcrysgrow.2013.09.001.

Nanev, C.N., Dimitrov, I.L., Hodzhaoglu, F.V., 2011. Growth of rhombohedral insulin crystals and in vitro modeling of their dissolution in the blood stream. Cryst. Res. Technol. 46, 119–126. https://doi.org/10.1002/crat.201000381.

Nanev, Christo N., Hodzhaoglu, F.V., Dimitrov, I.L., 2011. Kinetics of insulin crystal nucleation, energy barrier, and nucleus size. Cryst. Growth Des. 11, 196–202. https://doi.org/10.1021/cg1011499.

Nanev, C.N., Petrov, K.P., 2017. Steering a crystallization process to reduce crystal polydispersity; case study of insulin crystallization. J. Cryst. Growth 480, 164–169. https://doi.org/10.1016/j.jcrysgro.2016.11.068.

Nanev, C.N., Tonchev, V.D., 2015. Sigmoid kinetics of protein crystal nucleation. J. Cryst. Growth 427, 48–53. https://doi.org/10.1016/j.jcrysgro.2015.07.007.

Nanev, C.N., Tonchev, V.D., Hodzhaoglu, F.V., 2013. Protocol for growing insulin crystals of uniform size. J. Cryst. Growth 375, 10–15.

Nappo, V., Sullivan, R., Davey, R., Kuhn, S., Gavriilidis, A., Mazzei, L., 2018. Effect of shear rate on primary nucleation of para-amino benzoic acid in solution under different fluid dynamic conditions. Chem. Eng. Res. Des. 136, 48–56. https://doi.org/10.1016/j.cherd.2018.04.039.

Nielsen, L., Khurana, R., Coats, A., Frokjaer, S., Brange, J., Vyas, S., Uversky, V.N., Fink, A.L., 2001. Effect of environmental factors on the kinetics of insulin fibril formation: Elucidation of the molecular mechanism. Biochemistry 40, 6036–6046. https://doi.org/10.1021/bi002555c.

Norrman, M., Schluckebier, G., 2007. Crystallographic characterization of two novel crystal forms of human insulin induced by chaotropic agents and a shift in pH. BMC Struct. Biol. 7 (1), 14. https://doi.org/10.1186/1472-6807-7-83.

Parambil, J.V., Schaepertoens, M., Williams, D.R., Heng, J.Y.Y., 2011. Effects of oscillatory flow on the nucleation and crystallization of insulin. Cryst. Growth Des. 11, 4353–4359. https://doi.org/10.1021/cg200158z.

Penkova, A., Dimitrov, I., Nanev, C., 2004. Nucleation of insulin crystals in a wide continuous supersaturation gradient. Ann. N. Y Acad. Sci. 1027, 56–63. https://doi.org/10.1196/annals.1324.006.

Penkova, A., Pan, W., Hodjaoglu, F., Vekilov, P.G., 2006. Nucleation of protein crystals under the influence of solution shear flow. Ann. N. Y. Acad. Sci. 1077, 214–231. https://doi.org/10.1196/annals.1362.048.

Pereira, F.J.D., 2017. Numerical Optimization of an Oscillatory Flow Meso Reactor. University of Porto, Porto, Portugal.

Price, W.N., Chen, Y., Handelman, S.K., Neely, H., Karlin, R., Nair, R., Liu, J., Baran, M., Tong, S.N., Forouhar, F., Swaminathan, S.S., Xiao, R., Luft, J.R., Lauricella, A., Detitta, G.T., Rost, B., Montelione, G.T., Hunt, J.F., 2010. Understanding the physical properties controlling protein crystallization. Nat. Biotechnol. 27, 51–57. https://doi.org/10.1038/nbt.1514.Understanding.

Puhl, S., Meinel, L., Germershaus, O., 2016. Recent advances in crystalline and amorphous particulate protein formulations for controlled delivery. Asian J. Pharm. Sci. 11, 469–477. https://doi.org/10.1016/j.ajps.2016.06.003.

Reviakine, I., Georgiou, D.K., Vekilov, P.G., 2003. Capillarity effects on crystallization kinetics: Insulin. J. Am. Chem. Soc. 125, 11684–11693. https://doi.org/10.1021/ja030194t.

Roberts, M.M., Heng, J.Y.Y., Williams, D.R., 2010. Protein crystallization by forced flow through glass capillaries: enhanced lysozyme crystal growth. Cryst. Growth Des. 10, 1074–1083. https://doi.org/10.1021/cg900492j.

Roque, A.C.A., Pina, A.S., Azevedo, A.M., Aires-Barros, R., Jungbauer, A., Di Profio, G., Heng, J.Y.Y., Haigh, J., Ottens, M., 2020. Anything but conventional chromatography approaches in bioseparation. Biotechnol. J. 15, 1–8. https://doi.org/10.1002/biot.201900274.

Rossi, D., Gavriilidis, A., Kuhn, S., Candel, M.A., Jones, A.G., Price, C., Mazzei, L., 2015. Adipic acid primary nucleation kinetics from probability distributions in droplet-based systems under stagnant and flow conditions. Cryst. Growth Des. 15, 1784–1791. https://doi.org/10.1021/cg501836e.

Sheridan, R., Cardona, J., Tachtatzis, C., Chen, Y.C., Cleary, A., Briggs, N., Florence, A., Atkinson, R., Michie, C., Andonovic, I., Sefcik, J., 2022. Effect of oscillatory flow conditions on crystalliser fouling investigated through non-invasive imaging. Chem. Eng. Sci. 252, 1. https://doi.org/10.1016/j.ces.2021.117188.

Shi, D., Mhaskar, P., El-Farra, N.H., Christofides, P.D., 2005. Predictive control of crystal size distribution in protein crystallization. Nanotechnology 16, S562–S574. https://doi.org/10.1088/0957-4484/16/7/034.

Shiau, L.D., 2022. Comparison of the nucleation kinetics obtained from the cumulative distributions of the metastable zone width and induction time data. Molecules 27, 1–10. https://doi.org/10.3390/molecules27093007.

Stroobants, S., Callewaert, M., Krzek, M., Chinnu, S., Gelin, P., Ziemecka, I., Lutsko, J.F., De Malsche, W., Maes, D., 2020. The influence of shear on protein crystallization under constant shear conditions. Cryst. Growth Des. 20, 1876–1883. https://doi.org/10.1021/acs.cgd.9b01584.

Tait, S., White, E.T., Litster, J.D., 2009. A study on nucleation for protein crystallization in mixed vessels. Cryst. Growth Des. 9, 2198–2206.

Tonchev, V.D., Nanev, C.N., 2013. Growth and dissolution of equally-sized insulin crystals. Cryst. Res. Technol. 48, 1003–1010. https://doi.org/10.1002/crat.201300222.

Tsekova, D.S., 2009. Formation and growth of tetragonal lysozyme crystals at some boundary conditions. Cryst. Growth Des. 9, 1312–1317. https://doi.org/10.1177/1094428116641191.

Vekilov, P.G., 2007. What is the molecular-level role of the solution components in protein crystallization? Cryst. Growth Des. 7, 2239–2246. https://doi.org/10.1021/cg700989p.

Wang, L.B., Wakayama, N.I., Tao, W.Q., 2008. The role of solutal convection in protein crystal growth - a new dimensionless number to evaluate the effects of convection on protein crystal growth. J. Cryst. Growth 310, 5370–5374. https://doi.org/10.1016/j.jcrysgro.2008.09.125.

Wei, G., Su, Z., Reynolds, N.P., Arosio, P., Hamley, I.W., Gazit, E., Mezzenga, R., 2017. Self-assembling peptide and protein amyloids: from structure to tailored function in nanotechnology. Chem. Soc. Rev. 46, 4661–4708. https://doi.org/10.1039/c6cs00542j.

WHO. World Health Statistics [WWW Document], 2023. URL ⟨https://www.who.int/publications/i/item/9789240074323⟩ (accessed 01.01.2024).

Yang, H., Yu, X., Raval, V., Makkawi, Y., Florence, A., 2016. Effect of oscillatory flow on nucleation kinetics of butyl paraben. Cryst. Growth Des. 16, 875–886. https://doi.org/10.1021/acs.cgd.5b01437.

Yaoi, M., Adachi, H., Takano, K., Matsumura, H., Inoue, T., Mori, Y., Sasaki, T., 2004. Effect of stirring method on protein crystallization. Jpn. J. Appl. Phys. 43, 1318.